Integrated electricity and gas system modelling with hydrogen injections and gas composition tracking

Isam Saedi [*], Sleiman Mhanna, Pierluigi Mancarella

The University of Melbourne, Melbourne 3010, Australia

HIGHLIGHTS

- Integrated electricity, gas and hydrogen system modelling.
- Green hydrogen injections into the natural gas network and gas composition tracking.
- Identification of incoming and outgoing gas flow directions.
- Hydrogen molar fraction kept within limits during simultaneous injections.
- Real case study on Victorian electricity and gas transmission networks.

ARTICLE INFO

ABSTRACT

Despite the direct physical coupling between them, electricity and gas networks were traditionally modelled and operated independently. However, the heavy reliance on gas-fired generators to balance intermittent generation from renewable energy sources (RES), and the promising role of green hydrogen in decarbonising the natural gas system, have prompted a paradigm shift towards integrated electricity and gas system (IEGS) modelling. While many previous studies investigated the role of hydrogen in future low-carbon energy systems, a detailed assessment of hydrogen system integration into the electricity and gas transmission networks is still not addressed. Therefore, this paper presents a novel IEGS model with green hydrogen injections and gas composition tracking. The electricity system is modelled as a unit commitment model, formulated as a mixed-integer linear programming problem, and the gas system is modelled as a steady-state optimal gas flow (OGF). The developed model is demonstrated on two sets of case studies. The first case study validates the proposed OGF methodology on a small meshed gas test network, whereas the second case study demonstrates the applicability of the overall IEGS model with green hydrogen injection on the large-scale, real-world electricity and gas transmission networks of the state of Victoria (Australia). Results show that the proposed methodology can accurately capture the variations in gas flow direction while maintaining the hydrogen molar fraction within limits under hydrogen injections from multiple locations. Moreover, the amount of injected hydrogen not only depends on the level of RES curtailment, but also on local gas network constraints and local demand.

1. Introduction

Generally, electricity and gas networks are physically coupled primarily through gas-fired generators (GFG), electric compressors, and combined heat and power facilities. However, the advent of new clean fuel technologies, such as power-to-gas (PtG), will constitute an additional layer of coupling. The PtG process is viewed as an attractive and viable option for integrating renewable energy sources (RES) in large quantities, as it uses *green* energy from RES to produce hydrogen that can be then stored for later use. Hydrogen can also be blended with natural gas (NG) in existing NG pipelines, which represents a pathway for gas system decarbonisation. However, there are technical and safety challenges facing the injection of hydrogen into the existing NG network infrastructure. The technical issues are related to hydrogen embrittlement[1] [1] and the low energy content of hydrogen which can lead to greater linepack swings [2], whereas the safety-related issues associated

---

* Corresponding author.
  E-mail address: isaedi@student.unimelb.edu.au (I. Saedi).
[1] Mixing hydrogen with natural gas can weaken the mechanical strength of steel and increase the likelihood of corrosion.

with hydrogen are its wide range of flammability in air, low ignition point, high burning rate compared to other fuels, and invisible flame, all of which can lead to fire hazards [3]. However, blending hydrogen at low fractions should not lead to significant problems regarding household appliances, pipeline network integrity, and public safety in general [4].

Nonetheless, there are many advantages of injecting hydrogen into the NG network. In more detail, existing works on the impact of integrating PtG into the integrated electricity and gas system (IEGS), such as the ones in [5–7], developed transient gas-flow models to evaluate the ability of PtG to relieve gas pipeline constraints. In [5], the electricity and gas systems modelling is implemented in a multi-stage framework, and the changes in gas quality as a result of hydrogen injection were evaluated at a system level. However, evaluating changes in gas quality at a system level is applicable in scenarios when the same amount of hydrogen fraction is injected at every gas entry point in the gas network. Otherwise, the changes in gas quality should be evaluated at a nodal level. The work presented in [6] assessed the value of PtG through a combined electricity and gas system optimisation model under different hydrogen injection levels. However, the injected hydrogen was modelled as energy-equivalent NG flow rate. By the same token, the impact of hydrogen on gas quality cannot be captured. In [7], a probabilistic optimal power flow (OPF) of integrated electricity and gas system is used to overcome uncertainties from demand and wind power forecasting. However, the final product of a PtG unit was assumed to be synthetic natural gas (SNG), which possess similar properties to NG.

Moreover, [8] shows that PtG processes can enable RES to interact with existing (seasonal) storages, which has positive impacts on both gas and electricity networks. The hydrogen injection into the gas network was also considered, and the changes in gas quality were assessed at a system level. The positive impact of PtG on system security and RES integration is also highlighted in [9] with the help of robust optimisation techniques where the PtG is used to convert electricity to methane, whose properties are compatible with NG. On the other hand, [10] showcases the ability of PtG in providing flexibility, compared to electric storage and GFG, where the hydrogen volumetric flow rate produced by PtG was replaced by energy-equivalent NG flow rate. As a result, the impact of hydrogen injection on gas quality was neglected. Using electrolysers to provide flexibility to the electricity system is also analysed in [11], where the electrolysis units are used to absorb the RES energy that would otherwise be curtailed. The study showed that more utilization of generating assets can be achieved in the presence of flexible demand from electrolysers. However, no specific hydrogen end use was modelled in [11]. Furthermore, [12] presented a coupled electricity and gas model which shows that large quantities of synthetic methane can be stored and routed via GB's gas grids, which enables seasonal storage operations. The work in [13], implemented a security-constrained unit commitment model with hydrogen storage and demand response to improve the balance between energy production and consumption. The study only modelled the electricity system where the role of PtG is to produce hydrogen from excess wind energy and store it for later use to deliver energy to the electricity system via a hydrogen gas turbine.

To assess the impact of hydrogen injections, the hydrogen fraction needs to be tracked across the gas network under both steady-state and transient conditions. Under steady-state conditions, a gas flow model with gas quality tracking is used in [14–17] to assess the impact of alternative gases (biogas or hydrogen) injection into a gas network that is only supplied from a single NG supply point. In particular, [14] showcases how the injection of biogas into the gas distribution network can affect the Wobbe Index (WI), higher heating value (HHV), and relative density profiles across the system. The work developed in [15] assessed the impact of hydrogen and SNG injection on gas quality in a high-pressure gas network under non-isothermal conditions. Changes in the pressure profile and the WI as a result of hydrogen injection are investigated in [16] for a low-pressure distribution network in which hydrogen is injected under different percentages and up to 20 %mol. In

[17], both hydrogen and biogas injections into low-pressure gas distribution networks are assessed in terms of their impact on HHV, WI, and relative density.

Under transient conditions, gas flow is used to model the hydrogen injection and gas quality tracking in a multi-period framework. This allows the assessment of changes in gas quality when considering variable hydrogen injection profiles, as well as gas demand fluctuations. The work in [18,19] adopted isothermal transient modelling with hydrogen injection and quality tracking, whereas [20] used a non-isothermal transient flow modelling also in the presence of hydrogen injections. In these studies, the impact of hydrogen injection on gas quality is assessed in a single pipeline test system. However, recent work in [21], modelled the hydrogen injection for a 3-pipeline gas system, and under non-isothermal transient conditions. The above discussed studies on hydrogen injection and gas composition tracking did not consider the interaction with the electricity system, particularly in green hydrogen injection scenarios. This interaction, on the one hand, investigates the role of PtG in RES integration into the electricity system, and on the other hand, informs on the amount of energy that can be converted to hydrogen and then injected into the gas network. The work presented in [22] investigates the benefits of coupled electricity and gas systems under increasing penetration of solar PV generation where the hydrogen from excess solar PV is injected into the natural gas *distribution network*. The study solved the power and gas flow in radial distribution networks, and two hydrogen injection locations were assessed independently. A steady-state gas flow model is also used in [23] to analyse the impact of green hydrogen injection on low-pressure natural gas distribution systems. The green hydrogen is produced at the moments when power generated by RES exceeds the electricity demand. Different hydrogen injection locations were analysed independently to further understand the impact of hydrogen injection location on the gas mixture quality. Overall, using a gas flow modelling may have limitations in keeping the specified limit of hydrogen molar fraction in situations when hydrogen is injected simultaneously from different locations. Therefore, the approach in this paper uses the OGF to ensure hydrogen injection percentage is kept within the maximum limit.

In light of this background, there is a need to develop a modelling framework that can properly assess the role of green hydrogen injection in both the electricity and gas systems. In green hydrogen injections, the importance of considering the electricity system comes from the fact that the primary energy source for hydrogen production is determined by the operational characteristics of the electricity system. Likewise, implementing gas composition tracking on the gas system enables capturing the amount of hydrogen that can be injected as well as the changes in gas properties across the gas network as a results of hydrogen injection. The modelling framework should also be scalable in terms scenarios and applications. For instance, more complex hydrogen injection scenarios such as simultaneous distributed injections, nodal constraints on hydrogen molar fraction and constraints on RES energy availability should all be possible. Another important aspect is the implementation of such framework on real electricity and gas systems. This, in fact, not only provides a valuable insight into future energy system integration, but also demonstrates the applicability and scalability of the model on real-world problems. Therefore, this paper introduces an IEGS model with hydrogen injection (from curtailed RES electricity) and gas composition tracking. The proposed IEGS framework implements (i) a unit commitment (UC) model with a strengthened DC OPF [24] that incorporates transmission line losses, reserve requirements, ramp rates, and minimum up-and-down time constraints on generators, and (ii) a detailed steady-state OGF model with hydrogen injection and gas composition tracking that is suitable for capturing the amount of hydrogen injection and its impact on the gas system. The main contributions of this work are:

- To the best of our knowledge, the paper is the first to model green hydrogen injections into the gas network and gas composition
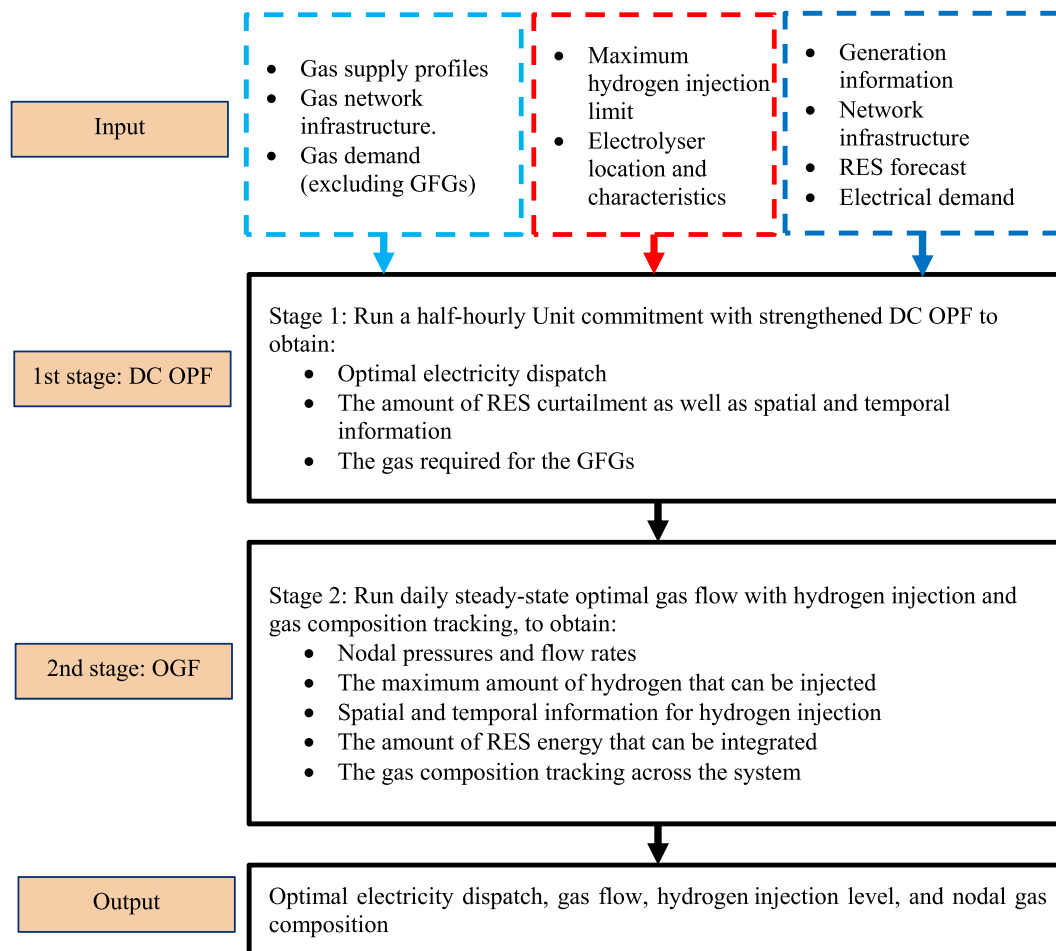
| Input | • Gas supply profiles
• Gas network infrastructure.
• Gas demand (excluding GFGs) | • Maximum hydrogen injection limit
• Electrolyser location and characteristics | • Generation information
• Network infrastructure
• RES forecast
• Electrical demand |

| 1st stage: DC OPF | Stage 1: Run a half-hourly Unit commitment with strengthened DC OPF to obtain:
• Optimal electricity dispatch
• The amount of RES curtailment as well as spatial and temporal information
• The gas required for the GFGs |

| 2nd stage: OGF | Stage 2: Run daily steady-state optimal gas flow with hydrogen injection and gas composition tracking, to obtain:
• Nodal pressures and flow rates
• The maximum amount of hydrogen that can be injected
• Spatial and temporal information for hydrogen injection
• The amount of RES energy that can be integrated
• The gas composition tracking across the system |

| Output | Optimal electricity dispatch, gas flow, hydrogen injection level, and nodal gas composition |

Fig. 1. The overall algorithmic approach.

tracking in the context of integrated electricity and gas transmission systems. This will highlight the importance of highly correlated temporal and geographical combined analysis of electricity and gas networks.

- Since gas composition tracking requires the accurate knowledge of gas flow directions, the paper presents a methodology to identify the correct gas flow directions regardless of the initial assumption on flow direction. As such, careful reformulations of gas mixing, gas flow, and node balance equations are proposed to account for unknown gas flow directions.
- The capabilities of the proposed model are demonstrated on case studies consisting of the *real* electricity and gas transmission networks of Victoria. In fact, previous works that modelled hydrogen injection with gas composition tracking are demonstrated on a gas system with a *single* NG source. However, real gas systems, like the Victorian one, feature multiple NG sources that supply NG to the system from different entry points, each with different gas compositions.
- Unlike previous studies which formulate the hydrogen injection and gas composition tracking as a *gas flow* problem, the current work formulates the problem as an *optimal gas flow* problem. This becomes more important in scenarios where hydrogen is injected simultaneously from different locations and there is a maximum injection limit that needs to be maintained at each node.

The modelling also assesses the profiles of water consumption, oxygen production and CO_2 emission reduction as a result of hydrogen production and injection.

The paper is structured as follows. Section 2 presents the overall

modelling methodology. The model is then validated in Section 3 with case studies involving the Victorian electricity and gas transmission networks. The paper concludes in Section 4.

2. Overall modelling methodology

This section describes the overall algorithmic methodology. A flow chart detailing this methodology is shown in Fig. 1. The input data consists mainly of the electricity and gas network infrastructures, electricity and gas demand profiles, RES forecasts, generation information, a predetermined percentage limit of hydrogen that can be injected into the gas network, location of hydrogen electrolysers and, more in general, injection points into the gas network. The first stage implements a UC with a strengthened DC OPF model solved over a 24-hour scheduling horizon with a half-hourly resolution. More details on the UC mathematical model can be found in Appendix B.1. Demand forecasts and RES availability forecasts are obtained from [25]. UC constraints on coal-fired generators include, minimum stable generation (MW), minimum up-time and down-time (hours), ramp rates (MW/hour), and reserve requirements (MW). These are all taken from [26]. The first stage determines the optimal dispatch of the generation mix and the amount and location of RES curtailments. The gas demand for GFG as well as RES curtailment are then used as input to the second stage. Generation outages and uncertainty in demand and renewable forecasts are considered through a reserve component. However, more complex models could be incorporated to the UC formulation in a straightforward way, such as implementing this algorithm in a receding horizon framework (model predictive control), as recently shown in [27] for example. Receding horizon approaches have in fact been proposed and
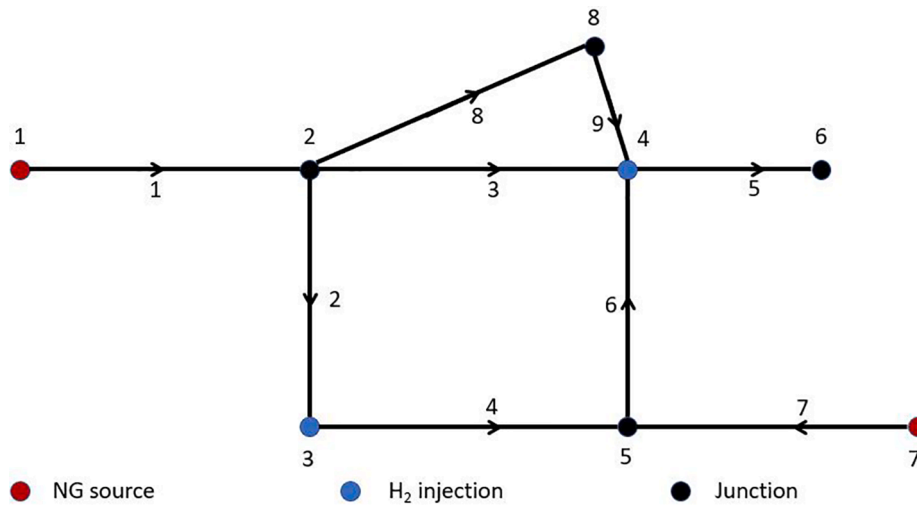
Fig. 2. 8-node illustrative gas system.

Table 1
Nodal gas demand.

Node	1	2	3	4	5	6	7	8
Energy Demand (MW)	250	360	600	320	580	300	250	950
Equivalent NG volumetric demand (m^3/s)	6.53	9.41	15.68	8.36	15.15	7.84	6.53	24.82

experimented with in closely related applications such as active distribution system management [28], generator dispatch control [29], and real-time price demand response [30], besides the aforementioned paper on multi-energy virtual power plant scheduling and dispatch [27].

The second stage consists of a steady-state OGF model with hydrogen injections and gas composition tracking, which determines the amount of hydrogen that can be injected into the gas system and its impact on the gas network operation. In fact, the molar composition of the gas mixture is determined at each gas node, which is then used to evaluate the gas properties and quality. The RES curtailments and the gas demands for gas-fired generators obtained from the first stage are averaged over the 24-hour scheduling horizon to be used as input to the second stage. The second stage optimisation solves the steady-state OGF under a time resolution of one day. In this work, it is assumed that, over the day, the gas system is in steady state conditions since at the end of the gas day, the total gas supply is balanced with the total gas demand to ensure sufficient linepack for the next day operation. Thus, this multi-scale temporal resolution not only strikes a good trade-off between analysis accuracy and computational efficiency, but is also deemed to adequately capture the characteristic operational time scales of both systems. A detailed mathematical formulation of the OGF model and the methodology of gas mixing equations is discussed in Appendices B.2 and B.3, respectively.

3. Case studies

The proposed model is demonstrated on two sets of case studies. The first case study is an illustrative example that consists of solving only the OGF model for an 8-node high pressure meshed gas network. The second case study implements the overall IEGS model on the real electricity and gas transmission networks of the state of Victoria.

3.1. Implementation setup

The developed model is written in Julia programming language [31] with JuMP is being used as a modelling language for the mathematical optimisation [32]. The MILP problem for the UC model is solved using

Gurobi solver [33], whereas the NLP problem for the OGF model is solved using IPOPT solver [34]. The programming is implemented on a computing platform with an Intel Core i7-8550U CPU at 1.8 GHz, and 16 GB RAM.

3.2. Case 1: 8-node illustrative example

In this section, the effectiveness of the proposed OGF methodology and the identification of incoming and outgoing gas flows that are necessary for gas composition tracking is demonstrated on an 8-node high-pressure gas system. The test system is depicted in Fig. 2, which shows the initial assumptions on gas flow directions. It consists of 8 nodes, 9 pipelines, 2 NG sources, and 2 hydrogen injection points. The minimum and maximum nodal pressures are 30 and 60 bar, respectively. The nodal gas demand is given in Table 1 and the network topology information is provided in Table 5 of Appendix C. The NG sources connected to nodes 1 and 7 have a maximum capacity (resp. supply cost) of 35 m^3/s (resp. 2.65 \$/GJ) and 60 m^3/s (resp. 2 \$/GJ), respectively. Both NG sources have molar compositions of 91.92% methane, 4.39% ethane, 0.53% propane, 0.09% butane, 0.76% nitrogen, 2.3% carbon dioxide and 0.0% hydrogen. The amount of injected hydrogen is only constrained by a maximum injection limit of 10 %vol.

The key findings of the Case 1 are tabulated in Table 2 and Table 3. As can be seen from Table 2, there is a reverse gas flow in pipelines 2, 4 and 9 as indicated by the negative flow rates. As a result, the actual gas flow direction (γ) becomes -1 for these pipelines. By utilising the values of γ, the direction of incoming and outgoing gas flows can be identified by evaluating μ and δ, where μ is equal to 1 if the actual flow direction matches the initial assumption of the gas flow direction in the pipeline and 0 otherwise, and δ is equal to 1 if the actual flow direction opposes the initial assumption of the gas flow direction in the pipeline and 0 otherwise (See Appendix B.3). Considering the nodal results given in Table 3, different gas compositions are witnessed at each gas node as a result of hydrogen injections as well as the gas mixture flow pattern. For example, we have zero hydrogen fractions at the NG supply nodes (as well as at node 5) due to NG flow stream, whereas a hydrogen fraction of 10% (the maximum limit) is witnessed at the hydrogen supply nodes, as

Table 2

Pipeline results of case 1: volumetric flow rate and gas flow directions.

Pipe	1	2	3	4	5	6	7	8	9
Flow rate (m^3/s)	26.12	−3.67	6.74	−18.42	8.40	19.92	53.48	13.57	−12.18
γ (-)	1	−1	1	−1	1	1	1	1	−1
μ (-)	1	0	1	0	1	1	1	1	0
δ (-)	0	1	0	1	0	0	0	0	1

Table 3

Node results of case 1: nodal pressure, relative density, calorific value, volumetric demand, and gas compositions.

Node	1	2	3	4	5	6	7	8
Pressure (bar)	38.43	31.83	31.99	31.24	36.07	30.72	56.47	30.00
Relative density (-)	0.606	0.600	0.552	0.552	0.606	0.552	0.606	0.577
CGV (MJ/m^3)	38.29	37.98	35.74	35.74	38.29	35.74	38.29	36.92
Actual volumetric demand (m^3/s)	6.53	9.48	16.79	8.96	15.15	8.40	6.53	25.74
Methane (%)	91.92	90.79	82.73	82.73	91.92	82.73	91.92	86.98
Ethane (%)	4.39	4.34	3.95	3.95	4.39	3.95	4.39	4.15
Propane (%)	0.53	0.52	0.48	0.48	0.53	0.48	0.53	0.50
Butane (%)	0.09	0.09	0.08	0.08	0.09	0.08	0.09	0.09
Nitrogen (%)	0.76	0.75	0.68	0.68	0.76	0.68	0.76	0.72
Carbone dioxide (%)	2.30	2.27	2.07	2.07	2.30	2.07	2.30	2.18
Hydrogen (%)	0.00	1.23	10.00	10.00	0.00	10.00	0.00	5.38

a) Electricity network of Victoria.
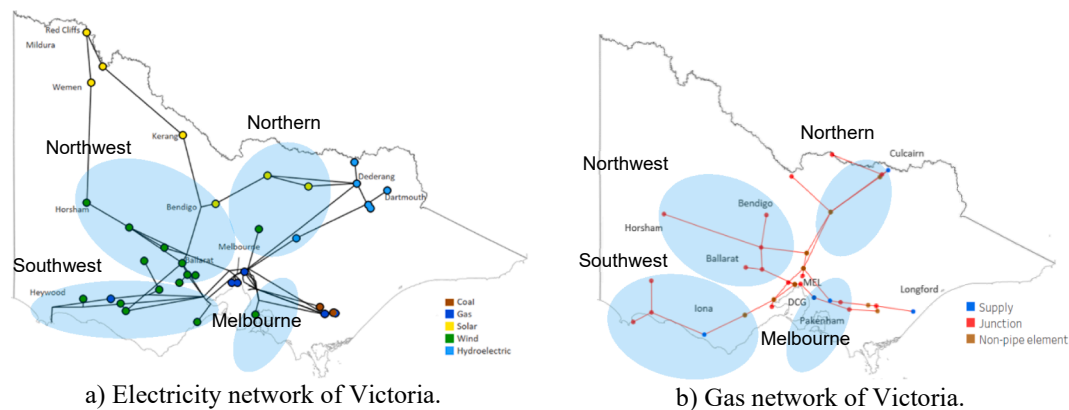

b) Gas network of Victoria.

Fig. 3. a) Electricity network, and b) Gas network of Victoria with the potential RES curtailment areas are shaded in blue.

well as at node 6. At those gas nodes where the hydrogen fraction is at its maximum, the relative density and gross calorific value (GCV) are at their minimum (due to the lower molecular weight and HHV of hydrogen, respectively). More specifically, the decrease in GCV leads the volumetric flow rate to increase in order to meet the energy demand. For instance, the volumetric gas demand at node 3 has increased from 15.68 m^3/s (as given in Table 1) to 16.79 m^3/s because of the reduction in the GCV. The effectiveness of the developed methodology for the gas composition tracking can also be appreciated by taking a closer look at the gas composition of node 8, for example. According to the initial gas flow direction assumption, node 8 has only one incoming flow (through pipeline 8) that is from node 2, which means that nodes 2 and 8 should have the same gas composition. However, as the gas flow in pipeline 9 (initially assumed to have an outgoing gas flow from node 8) is reversed, the model treats this pipeline as incoming to node 8. Therefore, the gas composition at node 8 and the corresponding gas properties are calculated as a result of mixing of 13.57 m^3/s (pipeline 8 flow rate with node 2 compositions) and −12.18 (pipeline 9 flow rate with node 4 compositions). Overall, in gas systems that are characterised by multiple NG sources that supply the NG to the system from different entry points, the injection of hydrogen from certain locations may not guarantee a consistent gas composition across the gas network. This inconsistency in gas composition leads to a nonuniform gas quality delivered to customers at different offtake nodes as has been seen from the GCV profiles

listed in Table 3. Therefore, the study also underscores the importance of gas composition tracking, which enables an accurate evaluation of gas quality at each node on the gas system. It is worth noting that the total volumetric gas supply from the NG sources at nodes 1 and 7 are 32.64 m^3/s and 60 m^3/s, respectively, whereas the hydrogen supplies flow rate injected at nodes 3 and 4 are 2.05 m^3/s and 2.87 m^3/s, respectively.

The importance of using OGF in keeping hydrogen fractions within the maximum limit in such hydrogen injection scenarios is also evident. For instance, the hydrogen injection locations for this network are connected through three possible paths which are, 3–2-4, 3-2-8–4 or 3–5-4. This in fact means that the hydrogen molar fraction injected in one location will affect the other injection location. Therefore, if gas flow were used to solve this problem instead of OGF, then we would need to run the model in many stages to keep the hydrogen molar fraction at 10%. More specifically, three stages are required to fully solve this specific problem, namely, (i) the first stage solves the gas flow with only NG to find the gas flow exchanged in each node in order to calculate the hydrogen volumetric flow rate that satisfies the 10% limit, (ii) the second stage solves the gas flow with NG and hydrogen injection at node 3 to find the gas flow exchanged and molar composition at each node in order to calculate the hydrogen volumetric flow rate that satisfies the 10% limit at node 4, and (iii) the third stage solves the final set of the gas flow problem with NG and hydrogen injection at nodes 3 and 4. Certainly, the more the hydrogen injection locations, the more stages
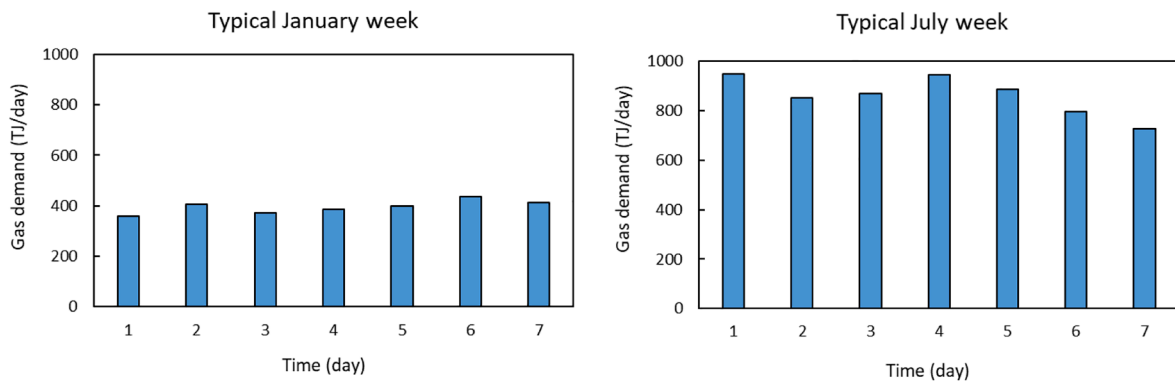
Fig. 4. Daily gas system demand (excluding GFG consumption) for a typical January week (left) and typical July week (right).
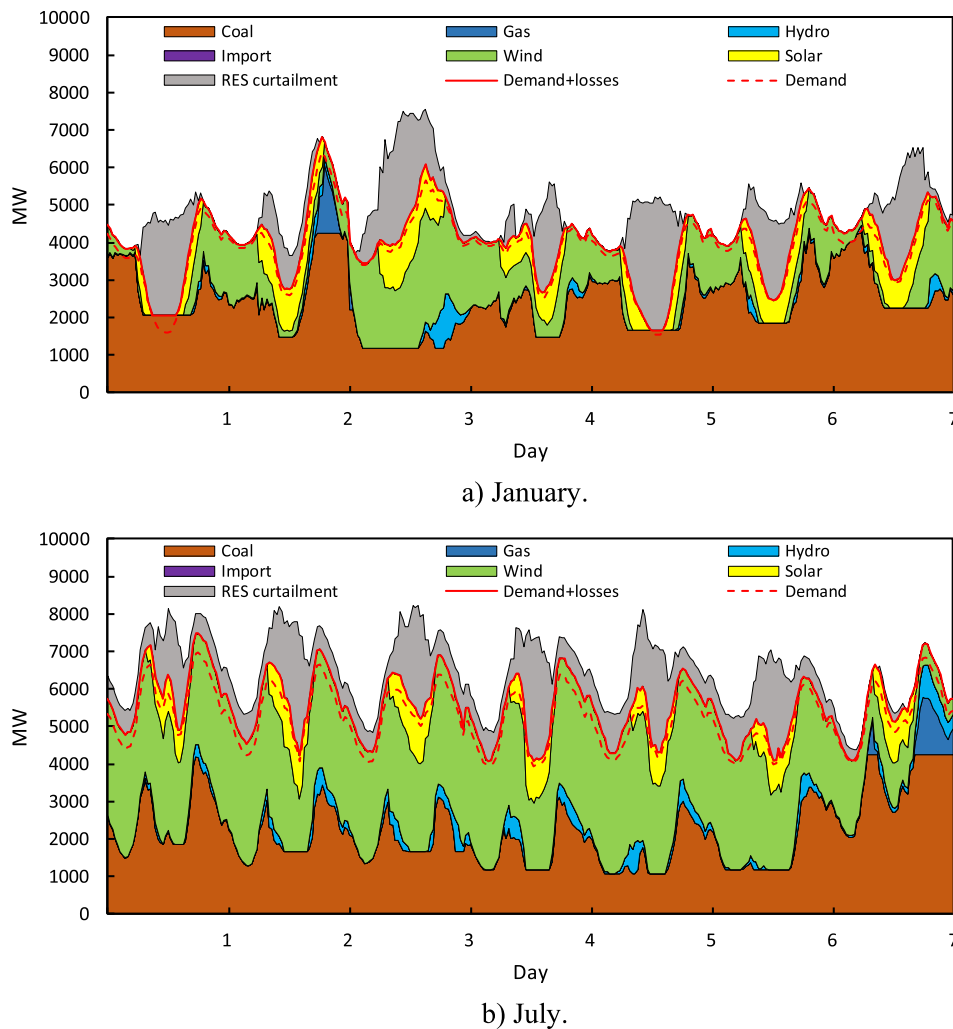

a) January.

b) July.

Fig. 5. Generation profile and RES curtailments for a) Representative week of January, and b) Representative week of July.

would be needed to solve the problem only using gas flow analysis. In contrast, OGF analysis allows a more straightforward, one-stage solution.

3.3. Case 2: Implementing the IEGS on Victorian energy system

The second case study implements the overall IEGS model on the Victorian electricity and gas transmission system and under the "Step Change" scenario of AEMO's integrated system plan [35] for representative summer and winter weeks in 2025. The Step change scenario considers future RES targets and plans regarding greenhouse gas emissions reduction by 2030. The case study highlights the importance of combined analysis of the electricity and gas networks in the presence of green hydrogen injections. The analysis includes an assessment of renewable energy curtailment due to network and system operating constraints and how more green energy could be overall incorporated in the system by allowing part of this curtailed energy to be recovered and transferred in the form of gas through hydrogen injection.

Fig. 6. RES energy curtailment in the four main curtailment areas in MWh/week for a) Representative week of January, and b) Representative week of July.
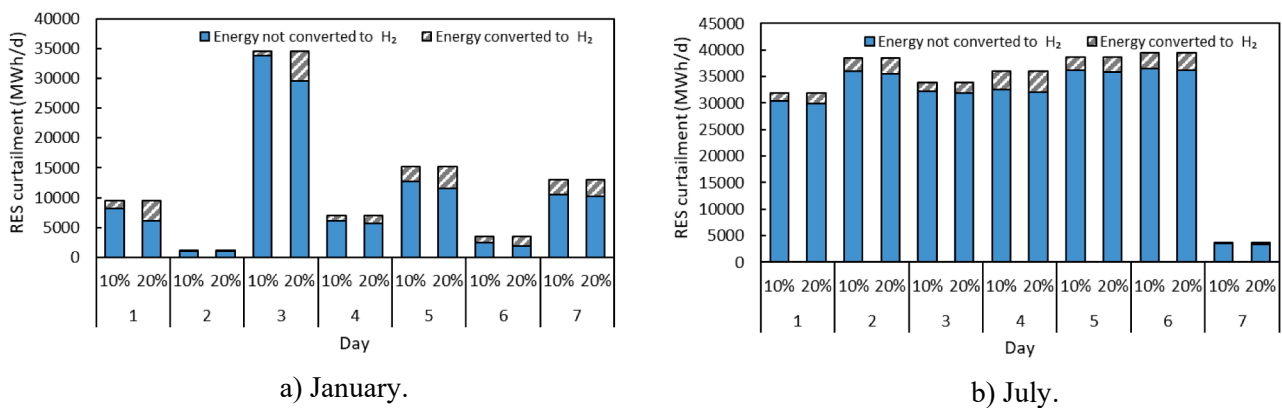

Fig. 7. Total RES energy curtailment converted/not converted to hydrogen for a) Representative week of January, and b) Representative week of July.
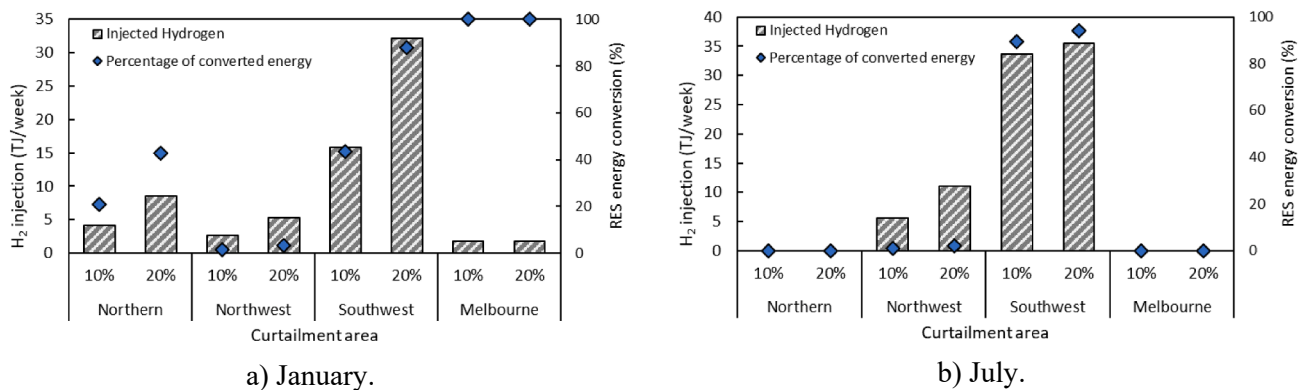

Fig. 8. Hydrogen injection along with the proportion of converted energy in the four main curtailment areas for a) Representative week of January, and b) Representative week of July.

Gas quality tracking is also included to account for additional operating constraints that might be relevant to network asset and appliances. We consider two predetermined percentages of possible hydrogen injection, namely, 10 %vol and 20 %vol, at the locations of RES curtailments. To deem green hydrogen injection feasible, the distance between an electrical bus with RES curtailment and the nearest gas node for candidate injection location is assumed to be at most 100 km. It is worth mentioning that although the case study is applied to the Victorian electricity and gas transmission systems, the methodology is completely general and can be applied to any electricity and gas systems.

3.3.1. Electricity and gas networks data

The electricity network data for transmission lines, transformers, buses, and generators is acquired from [36], and shown in Fig. 3(a). However, the data in [36] is updated to include the generation mix of 2025, and the augmentation of the interconnectors and transmission lines. The network consists of 81 buses, 135 transmission lines, 10 coal-fired units, 21 GFG, 26 wind turbine plants, 17 solar PV plants and 8 hydro-electric plants. The generation mix of 2025 is updated by including renewable energy zones generation outlook, obtained from [37], and the retirement of some coal-fired generators and GFG, obtained from [26]. The interconnectors and Western Victoria's electricity

Table 4

Total profiles of CO_2 emission reduction, oxygen production and water consumption.

Profile type	January		July	
	10% injection	20% injection	10% injection	20% injection
CO_2 emission reduction (tonnes)	1254.98	2452.67	2017.05	2386.06
Oxygen production (tonnes)	1293.32	2528.28	2079.24	2459.63
Water consumption (tonnes)	1627.63	3181.82	2621.13	3095.43

network are also augmented accordingly for 2025, as described in [26] and [38], respectively. The electricity demand and RES output forecasts for the corresponding scenario and representative days are obtained from [25].

The gas network model, the Victorian Declared Transmission System, was developed and validated with the help of industry support within the Future Fuels CRC project [39]. The network topology is shown in Fig. 3(b), and it consists of 48 nodes, 41 pipelines, 5 NG sources, 10 compressors and 7 pressure regulators. The gas network model in this work is updated to reflect the future pipeline augmentation and supply outlook identified in AEMO's Victorian Gas Planning Reports [40] and [41]. The daily gas demands for the representative winter and summer weeks are shown in Fig. 4. More details on available gas supply capacity and gas composition are provided in Appendix C. Finally, as the distance between an electrical bus with RES curtailment and the nearest gas node for candidate injection location was assumed to be at most 100 km, the potential RES curtailment locations on the electricity network can be aggregated into four main areas with 27 coupling points (PtG units). These four areas are identified in this work as Northern, Northwest, Southwest, and Melbourne. The mapping of these RES curtailment areas onto the gas network is depicted in Fig. 3(b).

3.3.2. Electricity system dispatch results

As discussed in Section 2, the first stage implements a UC with a strengthened DC OPF model solved over a 24-hour scheduling horizon with a half-hourly resolution. The generation profile with the total RES curtailment profile for the representative weeks of January and July are shown in Fig. 5(a) and Fig. 5(b), respectively. The representative week of July, which represents a typical winter week, has more wind availability compared to the representative week of January, which represents a typical summer week. In the Step scenario, the total installed capacity of wind and solar farms are 4301 MW and 1876 MW, respectively. However, despite the large availability of wind and solar capacities, curtailments are still substantial due to a combination of thermal limits on transmissions lines in these RES areas and reserve requirements from coal-fired generators. Fig. 6 gives the RES curtailment in MWh/week for each one of the four curtailment areas where the Northwest area witnesses the highest curtailment compared to other areas. The Northern and Melbourne areas have zero curtailed energy in July, whereas the Northwest and Southwest areas witness higher curtailment in July compared to January. The potential of converting the RES energy curtailment to hydrogen for injection into the gas network is assessed in the next section.

3.3.3. Assessing H_2 injection into the gas network

The daily curtailed energy from RES is shown in Fig. 7, which also shows the proportion of that curtailed energy that was converted to hydrogen and then injected into the gas network under 10 %vol and 20 %vol limits. As can be seen, when the injection percentage is increased to 20%, the amount of energy converted to hydrogen is doubled. However, a small proportion of the curtailed energy is converted to hydrogen and injected into the gas network mainly because of the constraints on

the injection limit. The total amount of injected hydrogen for each one of the four areas is depicted in Fig. 8, along with the percentage of energy converted to hydrogen. The Northwest area (where the highest RES curtailment is recorded) shows the lowest injected hydrogen compared to the total curtailed amount in this area. This is because most of the injection occurs in the offtake nodes where the hydrogen must be consumed locally and therefore cannot be transported to other parts of the gas network. In contrast, a higher proportion of energy curtailment is converted to hydrogen for injection in the remaining areas. For instance, the Southwest area accommodated more hydrogen injections compared to all the other areas except Melbourne and this is mainly because of its spatial characteristics in the gas network which allows more hydrogen to be blended with NG at higher volumes for the same %vol limit. The associated total water consumption, oxygen production, and CO_2 emission reduction profiles as a result of the hydrogen production and injection are shown in Table 4. The CO_2 emission reduction is evaluated in terms of the NG displacement in which the emission factor for NG is taken as 51.4 kg/GJ [42]. Table 4 shows that the larger level of hydrogen injection under 20 %vol leads to more water consumption, oxygen production and CO_2 emission reduction profiles. The above findings demonstrate how the IEGS modelling with hydrogen injection and gas composition tracking can, on the one hand, predict the level of RES energy curtailment on the electricity system, and, on the other hand, show how an insufficient capacity on the gas system may constrain the amount of curtailment converted to hydrogen for injection into the gas system.

3.4. Computational efficiency

Regarding the computational time, the first case study which runs a single snapshot OGF takes 0.154 s, the first stage of the second case study takes on average 14.505 s to run a 24-hour UC model with a 30-min resolution, and the second stage of the second case study takes on average 16.333 s to run a single snapshot OGF model. To improve computational efficiency, the active power, pressure and flow rate variables are non-dimensionalised using the base values of 100 MW, 10^6 Pa and 100 m^3/s, respectively.

4. Conclusion

This paper presented an integrated electricity and gas systems modelling with green hydrogen injection and gas composition tracking. The electricity system is modelled as a unit commitment problem with a strengthened DC OPF that accounts for electricity losses and technical constraints on generators, whereas the gas system is modelled as a steady-state optimal gas flow that can capture the amount of hydrogen injected and its impact on the gas system through the gas composition tracking. This detailed modelling of the two systems is aimed at capturing realistic operating constraints. In this work, we also introduce a methodology for identifying the incoming and outgoing gas flow directions to overcome the issue of unknown gas flow directions as well as a careful reformulation of gas mixing, gas flow and node balance equations. The developed model is demonstrated on two sets of case studies. The first case study shows the capabilities of the developed optimal gas flow methodology on an illustrative 8-node high-pressure meshed gas network. It has been shown that the developed model can capture the accurate incoming and outgoing gas flows regardless of initial assumptions on directions. Also, applying the optimal gas flow in situations when hydrogen is injected simultaneously from different locations can satisfy hydrogen fraction limit as well as gas network operating constraints. The second case study demonstrates the applicability of the proposed integrated electricity and gas systems model on real-world networks. In particular, this case study assesses the amount of hydrogen that can be injected in the Victorian gas network in areas close to where there may be renewable energy curtailment. It has been shown that the hydrogen production from curtailed renewable energy and its

subsequent injection into the gas network depends on the season, time of day, and location on the electricity and gas network. Therefore, this study underscores the importance of combined analysis of the electricity and gas networks by showing that while the amount of green hydrogen production depends on renewable energy curtailment through the spatio-temporal network-constrained assessment of the electricity system, the potential injection into the gas network ("power-to-gas") depends on the spatio-temporal availability of suitable gas flows to accommodate such injections according to the predefined maximum allowed %vol level.

Future work will focus on implementing the integrated electricity and gas systems analysis with hydrogen injection and gas composition tracking under transient conditions of the gas system. Moreover, ongoing work also includes the modelling of uncertainties by incorporating the unit commitment model in a receding horizon framework.

CRediT authorship contribution statement

Isam Saedi: Conceptualization, Methodology, Validation, Software,

Data curation, Writing – original draft, Visualization, Writing – review & editing. **Sleiman Mhanna:** Software, Data curation, Writing – review & editing, Supervision. **Pierluigi Mancarella:** Writing – review & editing, Supervision.

Declaration of Competing Interest

The authors declare that they have no known competing financial interests or personal relationships that could have appeared to influence the work reported in this paper.

Acknowledgments

Appendix A. Notation

Acronyms	
AEMO	Australian Energy Market Operator
GCV	Gross calorific value
GFG	Gas-fired generators
HHV	Higher heating value
IEGS	Integrated electricity and gas system
MILP	Mixed-integer linear programming
NG	Natural gas
NLP	Nonlinear programming
OGF	Optimal gas flow.
OPF	Optimal power flow
PtG	Power-to-gas
RES	Renewable energy sources
SNG	Synthetic natural gas
UC	Unit commitment
WI	Wobbe Index

Indices and sets	
i, j	Index of gas nodes.
ij	Index of pipelines, regulators and compressors, start from node i to node j.
m, n	Index of electrical buses.
mn	Index of transmission lines start from bus m to bus n.
g	Index of generators.
e	Index of power-to-gas units.
s	Index of natural gas supplies.
c	Index of molar fractions.
$\mathcal{N}$	Set of gas nodes.
$\mathcal{L}$	Set of gas pipelines.
ε	Set of all edges (i.e., pipelines, compressors and pressure regulators) in the gas network.
$\mathcal{C}$	Set of compressors.
$\mathcal{R}$	Set of pressure regulators.
$\mathcal{S}$	Set of natural gas supplies.
$\mathcal{P}$	Set of power-to-gas units.
$\mathcal{S}_i$	Set of gas suppliers connected to node i.
$\mathcal{H}_i$	Set of power-to-gas units connected to gas node i.
$\mathcal{P}_m$	Set of power-to-gas units connected to electricity bus m.
$\mathcal{B}$	Set of electrical Buses.
$\mathcal{B}_m$	Set of busses adjacent to bus m.
$\mathcal{I}$	Set of branches in electricity network.
$\mathcal{S}_i^{\mathrm{GFG}}$	Set of gas-fired units connected to gas node i.
$\mathcal{X}$	Set of molar compositions of gas mixture.
$\mathcal{T}$	Time horizon.
$\mathcal{G}^{\mathrm{C/G/RG}}$	Set of coal/ gas-fired/ renewable generators.
$\mathcal{G}_m^{\mathrm{C/G/RG}}$	Set of coal/ gas-fired/ renewable generators connected to bus m.

Constants	
L_{ij}	Pipeline length (m).
	Pipeline diameter (m).

(*continued on next page*)

(*continued*)

D_{ij}	
T	Gas temperature (K).
T^{st}	Gas temperature (288 K) at standard conditions.
p^{st}	Pressure (101325 Pa) at standard conditions.
R_{air}	Gas constant of air (287 J/kg.K)
M_c	Molecular weight (g/mol) of gas component c.
M^{air}	Molecular weight (29 g/mol) of air.
p^r, T^τ	Reduced pressure, temperature (-).
p^C	Critical pressure (Pa).
T^C	Critical temperature (K).
ω	Acentric factor (-).
P_m^d	Electrical power demand (MW) at bus m.
E_i^D	Gas energy demand (MJ/s) at node i.
f_{ij}	Friction factor (-).
η_{ij}	Pipeline efficiency (-).
η^{PtG}	Power to gas efficiency (-).
$\underline{\Delta\theta_{mn}}/\overline{\Delta\theta_{mn}}$	Lower/upper limit of voltage angle difference (rad) between bus m and n.
$\underline{\bullet}/\overline{\bullet}$	Minimum/Maximum operator.
RU_{gm}, RD_{gm}	Up/down ramp rate (MW/h) of coal-fired generator g at bus m.
g_{mn}	Line conductance (pu).
b_{mn}	Line susceptance (pu).
SR	Spinning reserve requirements (MW).
HHV_c	Higher heating value (MJ/m^3) for gas component c.
HHV^{H_2}	Higher heating value (12.75 MJ/m^3) of hydrogen.
GCV_s	Gross calorific value (MJ/m^3) of natural gas supplier s.
t	Time resolution (h)

Variables	
p_i	Pressure (Pa) at node i.
$\widetilde{p}_{ij}$	Average pressure (Pa) across edge ij.
q_{ij}	Gas volumetric flow rate (m^3/s) in edge ij.
q_{si}^S	Gas volumetric flow rate (m^3/s) from natural gas supply s at node i.
q_{ei}^{PtG}	Hydrogen volumetric flow rate (m^3/s) from power-to-gas unit e at node i.
E_{si}^S	Gas energy flow rate (MJ/s) from gas supply s at node i.
E_{ij}	Gas energy flow rate (MJ/s) in edge ij.
E_{ei}^{PtG}	Hydrogen energy flow rate (MJ/s) from power-to-gas unit e at node i.
E_{gi}^{GFG}	Energy demand (MJ/s) of GFG unit g at node i.
$P_{gm}^{C,G,RG}$	Active power (MW) generation of coal/gas-fired/renewable generator g at bus m.
P_{gm}^r	Spinning reserve (MW) from coal generator g at bus m.
θ_m	Bus voltage angle (rad) at bus m.
P_{mn}	Active power flow (MW) in transmission line mn.
Z_{ij}	Compressibility factor (-) in edge ij.
G_i	Relative density (-) at node i.
$x_{c,i}$	Molar fraction (-) of gas component c at node i.
r_{ij}	Pressure ratio (-) of a non-pipe element ij.
ΔP_{gm}	Power curtailments (MW) of RES unit g at bus m.
P_{em}^{PtG}	Electrical power input (MW) to a power-to-gas unit e at bus m.
GCV_i	Gross calorific value (MJ/m^3) at node i.
u_{gm}	Generator on or off status, equals 1 if unit gm is on, and 0 otherwise.
v_{gm}	Generator start-up, equals 1 only at the start-up of unit gm, and 0 otherwise.
w_{gm}	Generator shut-down, equals 1 only when unit gm is shut down, and 0. otherwise.

Appendix B. Mathematical modelling

This section details the mathematical modelling of the proposed IEGS with hydrogen injection and gas composition tracking. The first stage consists of a UC model with a strengthened DC OPF for the electricity system, whereas the second stage consists of a steady-state OGF model with hydrogen injections and gas composition tracking for the gas system.

B.1. Electricity system modelling

The electricity system model consists of a UC model with a strengthened DC OPF to determine the optimal dispatch of the generation mix, the RES curtailments, and the gas demands of the GFG. The DC OPF minimises the overall operational cost while satisfying the electricity demand subject to electricity transmission system constraints including network losses. All technical parameters are acquired from the Australian energy Market Operator (AEMO) [26]. The problem can be mathematically formulated as

$$\text{Min } f(P) = \sum_{t\in\mathscr{T}}\left(\sum_{gm\in\mathscr{Z}^C\cup\mathscr{Z}^G\cup\mathscr{Z}^{RG}} f_{gm}\left(P_{gm}^t\right)\right) \tag{1}$$

$$P_{gm} \leqslant P_{gm}^t \leqslant \overline{P}_{gm}, \quad gm \in \mathscr{G}^C \cup \mathscr{G}^G \cup \mathscr{G}^{RG}, \ t \in \mathscr{T} \tag{2}$$

$$-\overline{P}_{mn} \leqslant P_{mn}^t \leqslant \overline{P}_{mn}, \quad mn \in \mathscr{I}, \ t \in \mathscr{T} \tag{3}$$

$$\underline{\Delta\theta}_{mn} \leqslant \theta_m^t - \theta_n^t \leqslant \overline{\Delta\theta}_{mn}, \quad mn \in \mathscr{I}, \ t \in \mathscr{T} \tag{4}$$

$$\sum_{gm \in \mathscr{G}^C} P_{gm}^{r,t} \geqslant \text{SR}, \quad t \in \mathscr{T} \tag{5}$$

$$\sum_{g \in \mathscr{G}_m^C \cup \mathscr{G}_m^G \cup \mathscr{G}_m^{RG}} P_{gm}^t = P_m^{d,t} + \sum_{n \in \mathscr{B}_m} P_{mn}^t, \quad m \in \mathscr{B}, \ t \in \mathscr{T} \tag{6}$$

$$P_{mn}^t = g_{mn} 0.5 \left(\theta_{mn}^t\right)^2 + b_{mn}\theta_{mn}^t, \quad mn \in \mathscr{I}, \ t \in \mathscr{T} \tag{7}$$

$$P_{nm}^t = g_{nm} 0.5 \left(\theta_{mn}^t\right)^2 - b_{nm}\theta_{mn}^t, \quad nm \in \mathscr{I}^t, \ t \in \mathscr{T} \tag{8}$$

$$P_{gm}^t \leqslant u_{gm}^t \overline{P}_{gm}, \quad gm \in \mathscr{G}^C, \ t \in \mathscr{T} \tag{9}$$

$$P_{gm}^t \geqslant u_{gm}^t \underline{P}_{gm}, \quad gm \in \mathscr{G}^C, \ t \in \mathscr{T} \tag{10}$$

$$P_{gm}^t + P_{gm}^{r,t} \leqslant \overline{P}_{gm}, \quad gm \in \mathscr{G}^C, \ t \in \mathscr{T} \tag{11}$$

$$P_{gm}^t - P_{gm}^{t-1} \leqslant u_{gm}^{t-1} RU_{gm} + v_{gm}^t \underline{P}_{gm}, \quad gm \in \mathscr{G}^C, \ t \in \mathscr{T} \tag{12}$$

$$P_{gm}^{t-1} - P_{gm}^t \leqslant u_{gm}^t RD_{gm}, \quad gm \in \mathscr{G}^C, \ t \in \mathscr{T} \tag{13}$$

$$\sum_{t^{up}=t-\text{MUT}_{gm}+1} v_{gm}^{t^{up}} \leqslant u_{gm}^t, \quad gm \in \mathscr{G}^C, \ t \in \{\text{MUT}_{gm}, ..., \mathscr{T}\} \tag{14}$$

$$\sum_{t^{dn}=t-\text{MDT}_{gm}+1} w_{gm}^{t^{dn}} \leqslant 1 - u_{gm}^t, \quad gm \in \mathscr{G}^C, \ t \in \{\text{MDT}_{gm}, ..., \mathscr{T}\} \tag{15}$$

$$v_{gm}^t - w_{gm}^t \geqslant u_{gm}^t - u_{gm}^{t-1}, \quad gm \in \mathscr{G}^C, \ t \in \mathscr{T} \tag{16}$$

$$v_{gm}^t, w_{gm}^t \in [0,1], \ u_{gm}^t \in \{0,1\}, \quad gm \in \mathscr{G}^C, \ t \in \mathscr{T} \tag{17}$$

$$\Delta P_{gm}^t = \overline{P}_{gm}^t - P_{gm}^t, \quad gm \in \mathscr{G}^{RG}, \ t \in \mathscr{T} \tag{18}$$

$$P_{em}^{PtG,t} = \sum_{g \in \mathscr{P}_m} \Delta P_{gm}^t, \quad gm \in \mathscr{G}^{RG}, \ em \in \mathscr{P}, \ t \in \mathscr{T} \tag{19}$$

The objective function is described by (1) in which f_{gm} is the cost function of a generator unit. The limits on active power output from each generator are captured by (2). The active power and angle difference limits for transmission lines are captured by (3) and (4), respectively. The required spinning reserve is fulfilled according to (5). The spinning reserve is used to account for generation outages and uncertainty in demand and renewable forecasts [5,10]. Power balance at each bus is satisfied according to Kirchhoff's current law described by (6). The strengthened DC power flow constraints are given in (7) and (8) in which the line losses are approximated using the second-order Maclaurin series of the cosine function in the original AC OPF formulation, i.e., $\cos(\theta_{mn}) \approx 1 - 0.5(\theta_{mn})^2$, which gives a better approximation than the basic DC OPF counterpart. The ensuing nonlinear and nonconvex constraint is then approximated using piecewise linear segments [24]. The strengthened DC-OPF, which is taken from [24], is then extended to a UC model by incorporating the UC constraints given by (9)–(17), where (9)–(11) describe the active power limits for generating unit, whereas the ramping capabilities of coal-fired generating units are captured by (12) and (13). The minimum up-time and minimum down-time of a generating unit are captured by (14) and (15), respectively. More interestingly, since u_{gm}^t is binary, variables v_{gm}^t and w_{gm}^t can be modelled as continuous (as opposed to binary) thanks to constraint (16) which ensures that they take binary values in the solution. In more detail, if (16) is used to pivot w_{gm}^t out of the system given by (14) and (15), the resulting set defines the convex hull of the minimum up-time and down-time polytope on the space of variables u_{gm}^t and v_{gm}^t. The integrality constraint on the u_{gm}^t variables is described by (17). The power curtailment from each renewable generator is described by (18), which represents the difference between the forecast and dispatched power. Finally, the amount of electrical energy available for a PtG unit that may be connected to electricity bus m is equal to the sum of energy curtailment from RES units connected to that bus as described by (19). The resulting model is a mixed-integer linear programming (MILP) that can be solved efficiently using state-of-the-art industrial solvers.

B.2. Gas system modelling

This section describes the mathematical modelling of the gas system with hydrogen injections and gas composition tracking, which is used in the second stage of the overall algorithmic approach. The problem is formulated as a nonlinear OGF under steady-state conditions. The steady-state gas flow problem can be used to assess the daily operation of the gas system and the ability of the network to accommodate hydrogen gas. The problem described here gives a detailed modelling for the gas system, which considers the variation in the molar composition of the gas mixture as a result of hydrogen injection into the gas system. Therefore, the quality and properties of the gas mixture can be accurately captured across the gas network.

Recent studies on hydrogen injection and gas composition tracking have implemented a gas flow formulation which solves set of nonlinear

equations iteratively using for example the Newton-Raphson method. In gas flow problem, the number of unknown variables is balanced with the number of equations such that there are no free variables. For example, the hydrogen injection profiles could be specified, and we solve for hydrogen molar fraction, or vice versa. However, the solution for molar fraction may violate the maximum injection constraint or, the solution for hydrogen flow rate may violate the constraint on the available energy to produce hydrogen from otherwise curtailed RES. Therefore, the gas flow formulation may have limitations when it is implemented to solve a large-scale meshed gas network that has simultaneous hydrogen injection from different locations. Therefore, we formulated the problem as an OGF to have more control on hydrogen molar fraction, the available energy to produce hydrogen as well as the gas network operating constraints.

The gas demand is modelled as a constant energy offtake regardless of the hydrogen content. This entails that the corresponding volumetric gas demand increases as more hydrogen is blended into the gas system due to the lower HHV of hydrogen compared to NG. The hydrogen injection in this work is founded on the following premises:

- The gas flows in a horizontal pipeline and under steady-state isothermal conditions,
- The gas system is operating under normal conditions (e.g., no component outages, no isolations of specific parts of the network, etc.),
- Gas streams entering a node are perfectly mixed,
- It is possible to inject hydrogen into the gas network at a predefined volumetric percentage.

This OGF problem can be mathematically formulated as:

$$\text{Min } f(E) = \sum_{si\in\mathscr{S}} c_{si} E_{si}^{\text{S}} \tag{20}$$

$$\underline{p}_i \leqslant p_i \leqslant \overline{p}_i, \quad i \in \mathscr{N} \tag{21}$$

$$-\overline{q}_{ij} \leqslant q_{ij} \leqslant \overline{q}_{ij}, \quad ij \in \varepsilon \tag{22}$$

$$\underline{q}_{si}^{\text{S}} \leqslant q_{si}^{\text{S}} \leqslant \overline{q}_{si}^{\text{S}}, \quad si \in \mathscr{S} \tag{23}$$

$$q_{ij}^2 = \frac{\pi^2 R_{\text{air}}}{64}\left(\frac{T^{\text{st}}}{p^{\text{st}}}\right)^2 \frac{(p_i)^2 - (p_j)^2}{G_i L_{ij} T Z_{ij} f_{ij}} D_{ij}^5, \quad ij \in \mathscr{L} \tag{24}$$

$$G_i = \frac{\sum_{c\in\mathscr{X}} x_{c,i} M_c}{M_{\text{air}}}, \quad i \in \mathscr{N} \tag{25}$$

$$GCV_i = \sum_{c\in\mathscr{X}} x_{c,i} HHV_c, \quad i \in \mathscr{N} \tag{26}$$

$$\sum_{e\in\mathscr{H}_i} E_{ei}^{\text{PtG}} + \sum_{s\in\mathscr{S}_i} E_{si}^{\text{S}} + \sum_{ji\in\varepsilon} E_{ji} - \sum_{ij\in\varepsilon} E_{ij} = E_i^{\text{D}} + \sum_{g\in\mathscr{D}_i^{\text{GFG}}} E_{gi}^{\text{GFG}}, \quad i \in \mathscr{N} \tag{27}$$

$$x_{c,i} = \frac{\sum_{e\in\mathscr{H}_i} x_{c,ei} q_{ei}^{\text{PtG}} + \sum_{s\in\mathscr{S}_i} x_{c,si} q_{si}^{\text{S}} + \sum_{ji\in\varepsilon} x_{c,j} q_{ji}}{\sum_{e\in\mathscr{H}_i} q_{ei}^{\text{PtG}} + \sum_{s\in\mathscr{S}_i} q_{si}^{\text{S}} + \sum_{ji\in\varepsilon} q_{ji}}, \quad i,j \in \mathscr{N}, \ c \in \mathscr{X} \tag{28}$$

$$Z_{ij}^3 - Z_{ij}^2 + Z_{ij}(A_{ij} - B_{ij} - B_{ij}^2) - A_{ij}B_{ij} = 0, \quad ij \in \mathscr{L} \tag{29}$$

$$A_{ij} = 0.42747 \frac{\widetilde{p}_{ij}}{T^2}\left(\sum_{c\in\mathscr{X}} \frac{x_c T_c^{\text{C}} \alpha_c^{0.5}}{(p_c^{\text{C}})^{0.5}}\right)^2, \quad B_{ij} = 0.08664 \frac{\widetilde{p}_{ij}}{T} \sum_{c\in\mathscr{X}} \frac{x_c T_c^{\text{C}}}{p_c^{\text{C}}}, \quad ij \in \mathscr{L} \tag{30}$$

$$\alpha_c^{0.5} = 1 + (0.48 + 1.574\omega_c - 0.176\omega_c^2)\cdot\left(1 - \sqrt{\frac{T}{T_c^{\text{C}}}}\right), \quad c \in \mathscr{X} \tag{31}$$

$$\widetilde{p}_{ij} = \frac{2}{3}\left(p_i + p_j - \frac{p_i p_j}{p_i + p_j}\right), \quad ij \in \mathscr{L} \tag{32}$$

$$p_j = r_{ij} p_i, \quad ij \in \mathscr{C} \cup \mathscr{R} \tag{33}$$

$$\underline{r}_{ij} \leqslant r_{ij} \leqslant \overline{r}_{ij}, \quad ij \in \mathscr{C} \cup \mathscr{R} \tag{34}$$

$$q_{ij}(r_{ij} - 1) \leqslant 0, \quad ij \in \mathscr{R} \tag{35}$$

$$q_{ij}(1 - r_{ij}) \leqslant 0, \quad ij \in \mathscr{C} \tag{36}$$

$$E_{gi}^{\text{GFG}} = \frac{\sum_t P_{gm}^t}{\eta_{lgm}^{\text{GFG}}}, \quad gi \in \mathscr{D}^{\text{GFG}}, \ gm \in \mathscr{G}^{\text{G}} \tag{37}$$

$$\overline{E}_{ei}^{\text{PtG}} = \sum_t \eta^{\text{PtG}} P_{em}^{\text{PtG},t}, \quad ei \in \mathscr{H}_i, \ em \in \mathscr{P} \tag{38}$$

$$0 \leqslant E_{ei}^{\mathrm{PtG}} \leqslant \overline{E}_{ei}^{\mathrm{PtG}}, \quad ei \in \mathscr{H}_{\mathrm{i}} \tag{39}$$

$$x_{c,i} \leqslant \overline{x_{c,i}}, \quad i \in \mathscr{N}, \ c \in \mathscr{X}^{\mathrm{H_2}} \tag{40}$$

The objective function for the gas system is represented by (20), which finds the least-cost NG dispatch. The hydrogen is assumed to have a zero cost, which means that the amount of hydrogen injected is constrained by the availability of RES energy curtailment, the maximum limit on injection percentage, and/or gas network operating constraints. The limits on nodal pressure and pipe flow rate are captured by (21) and (22), respectively, whereas the gas supply limits are given by (23). Gas flow through a pipeline is described by the general flow equation (24), whereas the friction factor is described by $1/\sqrt{f_{ij}} = 20.64\eta_{ij}(D_{ij})^{1/6}$ according to Weymouth's definition [43]. The relative density and gross calorific value are evaluated based on molar composition at each node as described by (25) and (26), respectively. Energy balance at each node is given in (27), which guarantees that the energy demand is satisfied regardless of hydrogen content of the mixture where the conversion between the energy and volumetric flow rates is achieved by $E = GCV \cdot q$. The molar composition tracking is evaluated by (28), which assumes a perfect mix of incoming flows at node i. The compressibility factor, which describes the deviation of the real gas from the ideal gas, is described by Soave-Redlich-Kwong equation of state (29)–(31) [44]. The average pressure across a pipe is described by (32). The operation of non-pipe elements (i.e., compressors and pressure regulators) is delineated by (33)–(36), where (33) describes the boost (drop) of pressure by compressors (pressure regulators), (34) captures the limit on pressure ratio, and (35) and (36) forces the pressure ratio to become 1 during reverse flow through the pressure regulators and compressors, respectively. Note that $0 < \underline{r}_{ij}, \overline{r}_{ij} \leqslant 1$ for pressure regulators, and $\underline{r}_{ij}, \overline{r}_{ij} \geqslant 1$ for compressors. The gas energy demand required by GFG units connected to gas node i is described by (37), where the summation is over the time periods of one day. Likewise, the available energy that could be injected in the form of hydrogen gas from a PtG unit connected to node i is described by (38). The limits on hydrogen injection are captured by (39) and (40), where (39) enforces the injection limits based on the available energy from RES curtailment, while (40) enforces the injection limits based on the required volumetric percentage of hydrogen blending in the gas network. The above mathematical modelling of the gas system with hydrogen injection and gas composition tracking is suitable when the gas flow directions are known or fixed. Specifically, in gas composition tracking problem, the incoming and outgoing flow rates for a gas node i should be identified in order to solve the gas flow, node balance, and gas mixing equations described in (24), (27) and (28), respectively. However, in real gas systems where multiple gas sources inject NG into the system from different entry points as well as highly interconnected pipe and non-pipe elements, it is challenging to determine gas flow directions beforehand. Therefore, in this work, a methodology to overcome this issue is discussed in more detail in the next section.

B.3. Modelling of mixing equations

Injecting hydrogen into the NG network leads to variations in gas composition throughout the gas network. This diversity in the gas composition depends on how much hydrogen is injected as well as the injection location. The latter can be implemented in two scenarios: injection in the offtake nodes in which the NG-H$_2$ is consumed locally if hydrogen is injected at low percentages, and injection in the NG stream nodes in which the NG-H$_2$ mixture travels to other parts of the network depending on the flow direction of the mixture. Therefore, tracking gas composition is essential in the presence of hydrogen injection to ensure capturing the changes in gas quality and properties. However, one of the key challenges of gas composition tracking is identifying the pipelines with gas flows that may enter or leave a gas node in order to perform accurate gas mixing calculations. Here, we present a methodology that can handle the unknown flow directions by ensuring that the correct incoming/outgoing flow is captured.

For a gas node i the incoming and outgoing flows can be defined as,

$$\text{incoming flow} = \left\{ \begin{array}{l} j \to i, \text{ if } q_{ji} \geqslant 0 \\ i \to j, \text{ if } q_{ij} < 0 \end{array} \right\} \tag{41}$$

$$\text{ougoing flow} = \left\{ \begin{array}{l} j \to i, \text{ if } q_{ji} < 0 \\ i \to j, \text{ if } q_{ij} \geqslant 0 \end{array} \right\} \tag{42}$$

The positive terms in (41) and (42) are the ones that match the initial assumption of the flow direction based on the node-edge incidence matrix, whereas the negative terms are the ones that oppose the initial assumption on the flow direction. Therefore, the aim is to distinguish between the different flow directions in order to ensure the correct mixing of flow occurs in gas nodes. The formulation of the flow equation described in (24) is modified by including the absolute value of flow rate to allow for a bidirectional gas flow as given in (43). The information from (43) can then be used to evaluate the actual flow directions while solving the problem as written in (44)

$$q_{ij}|q_{ij}| = \frac{\pi^2 R_{\mathrm{air}}}{64} \left(\frac{T^{\mathrm{st}}}{p^{\mathrm{st}}} \right)^2 \frac{(p_i)^2 - (p_j)^2}{G_i L_{ij} T Z_{ij} f_{ij}} D_{ij}^5, \quad ij \in \mathscr{L} \tag{43}$$

$$\gamma_{ij} = \mathrm{sign}(q_{ij}), \quad ij \in \varepsilon \tag{44}$$

where γ_{ij} is the actual flow direction of edge ij. The flow direction described in (44) can also be written as:

$$\gamma_{ij} = \frac{q_{ij}}{|q_{ij}|}. \quad ij \in \varepsilon \tag{45}$$

As the actual flow direction is now known for each edge in the gas network, it is possible to identify the correct incoming and outgoing flows. This can be achieved using the following definitions,

$$\mu_{ij} = 0.5 \left(|\gamma_{ij}| + \gamma_{ij} \right), \quad ij \in \varepsilon \tag{46}$$

$$\delta_{ij} = 0.5 \left(|\gamma_{ij}| - \gamma_{ij} \right), \quad ij \in \varepsilon \tag{47}$$

where μ_{ij} is equal to 1 if the actual flow direction matches the initial assumption of the gas flow direction in the edge ij and 0 otherwise, and δ_{ij} is equal to 1 if the actual flow direction opposes the initial assumption of the gas flow direction in the edge ij and 0 otherwise. The definitions described in

(46) and (47) are also used in [15] to define the gas flow that enters or leaves a gas node from external environments (i.e., supply or demand). However, in this work, these definitions are further extended to identify the edges with incoming and outgoing flows. Then, they are further used to reformulate the equations that require accurate knowledge of flow directions. Thus, (27) and (28) are rewritten as

$$
\sum_{e \in \mathcal{H}_i} q_{ei}^{PtG} HHV^{H_2} + \sum_{s \in \mathcal{S}_i} q_{si}^{S} GCV_s + \sum_{ji \in \varepsilon} \mu_{ji} q_{ji} GCV_j - \sum_{ij \in \varepsilon} \mu_{ij} q_{ij} GCV_i +
$$
$$
\sum_{ji \in \varepsilon} \delta_{ji} q_{ji} GCV_i - \sum_{ij \in \varepsilon} \delta_{ij} q_{ij} GCV_j = E_i^{D} + \sum_{g \in \mathcal{S}_i^{GFG}} E_{gi}^{GFG}, \quad i \in \mathcal{N}
$$
(48)

$$
x_{c,i} = \frac{\sum_{e \in \mathcal{H}_i} x_{c,ei} q_{ei}^{PtG} + \sum_{s \in \mathcal{S}_i} x_{c,si} q_{si}^{S} + \sum_{ji \in \varepsilon} \mu_{ji} x_{c,j} q_{ji} - \sum_{ij \in \varepsilon} \delta_{ij} x_{c,j} q_{ij}}{\sum_{e \in \mathcal{H}_i} q_{ei}^{PtG} + \sum_{s \in \mathcal{S}_i} q_{si}^{S} + \sum_{ji \in \varepsilon} \mu_{ji} q_{ji} - \sum_{ij \in \varepsilon} \delta_{ij} q_{ij}}. \quad i,j \in \mathcal{N}, \ c \in \mathcal{X}
$$
(49)

Likewise, the general gas flow equation described in (43) is also updated to ensure the upstream relative density is always selected regardless of changes in the gas flow direction:

$$
q_{ij} |q_{ij}| = \frac{\pi^2 R_{air}}{64} \left(\frac{T^{st}}{p^{st}} \right)^2 \frac{(p_i)^2 - (p_j)^2}{(\mu_{ij} G_i + \delta_{ij} G_j) L_{ij} T Z_{ij} f_{ij}} D_{ij}^5. \quad ij \in \mathcal{L}
$$
(50)

The formulation in (48)–(50) will ensure that accurate gas flow directions are captured regardless of initial assumptions on directions. This form of gas composition tracking can be used in both gas flow and optimal gas flow problems.

Appendix C. Case studies input data

See Tables 5-7

Table 5
Gas network topology for case study 1.

Pipeline	From node	To node	Length (km)	Diameter (m)
1	1	2	50	0.4
2	2	3	60	0.4
3	2	4	60	0.4
4	3	5	60	0.4
5	4	6	36	0.4
6	5	4	60	0.4
7	7	5	50	0.4
8	2	8	45	0.4
9	8	4	40	0.4

Table 6
Forecast of Victorian gas system supply adequacy for 2024 [41,45].

Supply zone	Capacity (TJ/d)
Gippsland[1]	651
Port Campbell[2]	449
Dandenong LNG	87
Total available	1187

[1] The supply in the Gippsland zone is the aggregated gas supply from Longford CPP and Pakenham.
[2] The supply in the Port Campbell zone is the aggregated gas supply from Iona UGS, Otway, and Minerva.

Table 7
Victorian NG supply composition [46].

Gas components	Gas supply point				
	Longford (%vol)	Pakenham (%vol)	Port Campbell (%vol)	Dandenong LNG (%vol)	Culcairn (%vol)
Methane	91.92	86.27	91.56	92.12	97.7
Ethane	4.39	7.01	3.88	4.304	0.63
Propane	0.53	1.21	0.46	0.427	0.07
I-butane	0.09	0.27	0.13	0.03	0.02
Nitrogen	0.76	0.5	1.54	0.756	1.12
Carbon dioxide	2.3	4.72	2.33	2.275	0.45
Hydrogen	0	0	0	0	0

References

[1] Altfeld K, Pinchbeck D. Admissible hydrogen concentrations in natural gas systems. Gas Energy 2013;March/2013:1–16.

[2] D. Haeseldonckx and D. William, The use of the natural-gas pipeline infrastructure for hydrogen transport in a changing market structure, 32, 1381–1386, 2007.

[3] Stolecka M. Hazards of hydrogen transport in the existing natural gas pipeline network. J. Power Technol. 2018;98(4):329–35.

[4] Melaina M, Antonia O, Penev M. Blending Hydrogen into Natural Gas Pipeline Networks: A Review of Key Issues. Contract 2013;303(March):275–3000.

[5] Clegg S, Mancarella P. Integrated Modelling and Assessment of the Operational Impact of Power-to-Gas (P2G) on Electrical and Gas Transmission Networks. IEEE Trans. Sustain. Energy 2015;6(4):1234–44.

[6] Qadrdan M, Abeysekera M, Chaudry M, Wu J, Jenkins N. Role of power-to-gas in an integrated gas and electricity system in Great Britain. Int. J. Hydrogen Energy 2015;40(17):5763–75.

[7] Sun G, Chen S, Wei Z, Chen S. Multi-period integrated natural gas and electric power system probabilistic optimal power flow incorporating power-to-gas units. J. Mod. Power Syst. Clean Energy 2017;5(3):412–23.

[8] Clegg S, Mancarella P. Storing renewables in the gas network: modelling of power-to-gas seasonal storage flexibility in low-carbon power systems. IET Gener. Transm. Distrib. 2015;10(3):566–75.

[9] He C, Liu T, Wu L, Shahidehpour M. Robust coordination of interdependent electricity and natural gas systems in day-ahead scheduling for facilitating volatile renewable generations via power-to-gas technology. J. Mod. Power Syst. Clean Energy May 2017;5(3):375–88.

[10] Qadrdan M, Ameli H, Strbac G, Jenkins N. Efficacy of options to address balancing challenges: Integrated gas and electricity perspectives. Appl. Energy 2017;190:181–90.

[11] Ruggles TH, Dowling JA, Lewis NS, Caldeira K. Opportunities for flexible electricity loads such as hydrogen production from curtailed generation. Adv. Appl. Energy 2021;3, no. June:100051.

[12] A. Antenucci and G. Sansavini, "Extensive CO2 recycling in power systems via Power-to-Gas and network storage," Renew. Sustain. Energy Rev., vol. 100, no. July 2018, pp. 33–43, 2019.

[13] Mirzaei MA, Sadeghi Yazdankhah A, Mohammadi-Ivatloo B. Stochastic security-constrained operation of wind and hydrogen energy storage systems integrated with price-based demand response. Int. J. Hydrogen Energy 2019;44(27):14217–27.

[14] Cavana M, Leone P. Biogas blending into the gas grid of a small municipality for the decarbonization of the heating sector. Biomass Bioenergy 2019;vol. 127, no. February:105295.

[15] S. Pellegrino, A. Lanzini, and P. Leone, "Greening the gas network – The need for modelling the distributed injection of alternative fuels," Renew. Sustain. Energy Rev., vol. 70, no. October 2015, pp. 266–286, 2017.

[16] Abeysekera M, Rees M, Wu J. Simulation and analysis of low pressure gas networks with decentralized fuel injection. Energy Procedia 2014;61:402–6.

[17] M. Abeysekera, J. Wu, N. Jenkins, and M. Rees, "Steady state analysis of gas networks with distributed injection of alternative gas q," vol. 164, pp. 991–1002, 2016.

[18] Guandalini G, Colbertaldo P, Campanari S. Dynamic modeling of natural gas quality within transport pipelines in presence of hydrogen injections. Appl. Energy 2017.

[19] Guandalini G, Colbertaldo P, Campanari S. Dynamic Quality Tracking of Natural Gas and Hydrogen Mixture in a Portion of Natural Gas Grid. Energy Procedia 2015;75:1037–43.

[20] Chaczykowski M, Zarodkiewicz P. Simulation of natural gas quality distribution for pipeline systems. Energy 2017;134:681–98.

[21] Osiadacz AJ, Chaczykowski M. Modeling and Simulation of Gas Distribution Networks in a Multienergy System Environment. Proc. IEEE 2020;108(9):1580–95.

[22] Cavana M, Mazza A, Chicco G, Leone P. Electrical and gas networks coupling through hydrogen blending under increasing distributed photovoltaic generation. Appl. Energy 2021;vol. 290, no. March:116764.

[23] Cheli L, Guzzo G, Adolfo D, Carcasci C. Steady-state analysis of a natural gas distribution network with hydrogen injection to absorb excess renewable electricity. Int. J. Hydrogen Energy 2021;46(50):25562–77.

[24] Dos Santos TN, Diniz AL. A dynamic piecewise linear model for DC transmission losses in optimal scheduling problems. IEEE Trans. Power Syst. 2011;26(2):508–19.

[25] Australian Energy Market Operator, "2020 Integrated System Plan database," 2020. [Online]. Available: https://aemo.com.au/energy-systems/major-publications/integrated-system-plan-isp/2020-integrated-system-plan-isp/2019-isp-database.

[26] Australian Energy Market Operator, "2019 Input and Assumptions workbook," 2019. [Online]. Available: https://aemo.com.au/-/media/files/electricity/nem/planning_and_forecasting/inputs-assumptions-methodologies/2019/2019-input-and-assumptions-workbook-v1-3-dec-19.xlsx?la=en.

[27] Naughton J, Wang H, Riaz S, Cantoni M, Mancarella P. Optimization of multi-energy virtual power plants for providing multiple market and local network services. Electr. Power Syst. Res. 2020;189(October 2019):106775.

[28] Saint-Pierre A, Mancarella P. Active Distribution System Management: A Dual-Horizon Scheduling Framework for DSO/TSO Interface under Uncertainty. IEEE Trans. Smart Grid 2017;8(5):2186–97.

[29] Venkat AN, Hiskens IA, Rawlings JB, Wright SJ. Distributed MPC strategies with application to power system automatic generation control. IEEE Trans. Control Syst. Technol. 2008;16(6):1192–206.

[30] Chen Z, Wu L, Fu Y. Real-time price-based demand response management for residential appliances via stochastic optimization and robust optimization. IEEE Trans. Smart Grid 2012;3(4):1822–31.

[31] Bezanson J, Edelman A, Karpinski S, Shah VB. Julia: A fresh approach to numerical computing. SIAM Rev. 2017;59(1):65–98.

[32] Dunning I, Huchette J, Lubin M. JuMP: A modeling language for mathematical optimization. SIAM Rev. 2017;59(2):295–320.

[33] Gurobi Optimization LLC, "Gurobi Optimizer Reference Manual," 2019. [Online]. Available: http://www.gurobi.com.

[34] Wächter A, Biegler LT. On the implementation of an interior-point filter line-search algorithm for large-scale nonlinear programming. Math. Program. 2006;106(1):25–57.

[35] Australian Energy Market Operator, "2020 Integrated System Plan," 2020.

[36] Xenophon A, Hill D. Open grid model of Australia's national electricity market allowing backtesting against historic data. Sci. Data 2018;5:1–21.

[37] Australian Energy Market Operator, "AEMO ISP 2020 - Renewable Energy Zones Generation Outlook," 2020. [Online]. Available: https://aemo.com.au/energy-systems/major-publications/integrated-system-plan-isp/2020-integrated-system-plan-isp/draft-2020-isp-archive.

[38] Australian Energy Market Operator, "Western Victoria Renewable Integration PCAR," 2019.

[39] "Future Fuels CRC." [Online]. Available: https://www.futurefuelscrc.com/.

[40] AEMO, "Victorian Gas Planning Report," 2019.

[41] Australian Energy Market Operator, "Victorian Gas Planning Report Update Gas Transmission Network Planning for Victoria," 2020.

[42] The Office of Parliamentary Counsel, "National Greenhouse and Energy Reporting (Measurement) Determination," 2008.

[43] A. Osiadacz, Simulation and analysis of gas networks. 1987.

[44] Soave G. Equilibrium constants from a modified Redlich-Kwong equation of state. Chem. Eng. Sci. 1972;27(6):1197–203.

[45] Australian Energy Market Operator, "Victorian Gas Planning Report," no. March, 2019.

[46] Australian Energy Market Operator, "Data (DWGM)." [Online]. Available: https://aemo.com.au/energy-systems/gas/declared-wholesale-gas-market-dwgm/data-dwgm.